Gas-Phase Pyrolysis of 1,3,3-Trinitroazetidine: Shock Tube Kinetics

Yi-Xue Zhang and S. H. Bauer*

Chemistry Department, Baker Chemical Laboratory, Cornell University, Ithaca, New York 14853

Received: January 28, 1998; In Final Form: May 11, 1998

Vapors of 1,3,3-trinitroazetidine (TNAZ) were pyrolyzed in a single-pulse shock tube, under high dilution in Ar, over the temperature range 750−1100 K (reflected shocks). The decay of TNAZ and the appearance of the reactive intermediate, NO_2, were followed spectrophotometrically at 271 and 405 nm, respectively, in real time via a multiple-pass quartz extension of the shock tube terminus. Samples of the major products that were generated during 1.5 ms residence time and wave quenched were identified and quantitated by GC and FTIR. The unimolecular rate constant (high-pressure limit) for dissociation of TNAZ under our experimental conditions is $k_{uni} = 10^{13.96\pm0.63} \exp[(-19900 \pm 1190)/T]$, s^{-1}. Successive fissions of NO_2 groups were indicated by the time-dependent absorption levels at 405 nm. A gas-phase FTIR spectrum of TNAZ recorded at ∼110 °C provided the missing data for computing the thermochemical parameters for this compound. Then the partition of its decomposition products (minimal free energy) could be calculated for 900 and 1100 K. The observed product distributions differ markedly from those calculated, indicating that the overall reaction is kinetically limited. Several possible reaction pathways at the early stages of the pyrolysis are discussed, and a preliminary reaction mechanism consisting of 46 chemical reactions is proposed. Simulations based on this mechanism agree reasonably well with the experimental results despite uncertainties. Additional work on the pyrolyses of mono- and dinitro substituted azetidines is needed to determine the relative importance of the various dissociation pathways in the present system.

Introduction

Extensive literature is now available covering numerous experiments that explored the physics and chemistry of high-energy materials.[1−3] RDX (hexahydro-1,3,5-trinitro-*s*-triazine) and HMX (1,3,5,7-tetranitro-1,3,5,7-tetraazacyclooctane) have received the most attention. Behrens and Bulusu[4] reported on the thermal decomposition sequences of these compounds, which they followed by thermogravimetric modulated-beam mass spectrometry, assisted by judicious use of isotopic labels. RDX generated a mixture of about a dozen identifiable compounds that ranged from diatomic species (CO) to poly-atomics (nitroso-*s*-traizine). Four pathways had to be postulated, two being unimolecular (HONO elimination and N−N bond fission), that were closely followed by reactions between intermediates generated during the initial stages. They also observed that the rate of decomposition increased significantly upon melting. The residence pyrolysis times for these cleverly designed experiments lasted from $^1/_2$ to 3 ms and covered the temperature range 460−485 K. They concluded, "Neither experiments with simple nitramines, nor molecular decomposition experiments, fully address the reaction mechanism that control the decomposition of RDX." Behrens[5] presented cartoons to call attention to the absence of adequate overlap between the operational space available for obtaining experimental information and conditions under which these materials are typically used.

The extended list of topics covered in the NATO ASI proceedings reveals the wide range of probes utilized in the exploration of highly energetic materials (HEMs). The occurrence of autocatalysis in generating secondary products, following initial molecular fragmentation, was clearly demonstrated in companion reports. Critical analysis of nitramine decompositions, wherein product distributions were summarized for RDX and HMX, as well as measured activation energies were listed by Schroeder.[6]

Much effort has been devoted to develop methods for calculating heats of formation, bond dissociation energies, and relative stabilities (both at ab inito and empirical levels) of HEMs (gas-phase species). The results proved particularly useful for guiding the synthesis of a wide variety of derivatives with attractive characteristics, such as high-energy density, low sensitivity to impact, ease of production, etc. The computational results merit direct cross-checking with measurements made for the corresponding gaseous species. Equally important, information on fragmentation processes at the molecular level (bond fission, activation energies; endo/exo thermicities) is needed to provide a basis for comparison with activation energies derived from solid/liquid-phase decompositions—so as to permit deconvolution of values that may be ascribed to specific molecular structure from contributions due to crystal field bonding and from induced (auto) catalyses developed when initial products of decomposition are trapped in the solid matrix.

1,3,3-trinitroazetidine (TNAZ) is a high-energy explosive, solid at room temperature, with a somewhat lower energy output than RDX. It is particularly attractive: because of its low sensitivity it is easily handled, and it is steam castable. Its melting point is 101 °C; density (xr) = 1.84 g/mL, and is thermally stable (240 °C).[7] An X-ray structure has been reported by Oyumi et al.[8] The frequencies of its infrared spectrum (solid) have been assigned.[8] The attractive utilitarian properties of TNAZ justify an extended exploration of its mechanism of fragmentation and, in particular, to establish the early sequence of loss of the NO_2 groups as well as break-up of the four-member ring. The unsubstituted azetidine fissions

S1089-5639(98)00931-1 CCC: $15.00
Published on Web 06/26/1998

in a single step:[9,10]

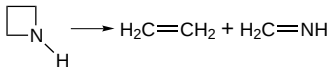

(R1)

$$k_{uni} = 9.54 \times 10^{14} \exp(-54800/RT),\ s^{-1}$$

However, in the (NO_2)-trisubstituted compound, weaker bonds are present that break with activation energies lower by 10−12 kcal/mol. Then the generated radical species continue to fragment, following an as yet undetermined sequence of steps.

A single-pulse shock tube, heatable to 150 °C, is an ideal tool for study of the pyrolysis of the gas phase under high Ar dilution. Rates of degradation of TNAZ and the appearance of NO_2 can be monitored in the μs regime by recording their time-dependent absorption spectra in the UV; samples of product species quenched after ∼1.5 ms (shock conditions) can be analyzed via GC or IR.

Experiments

The shock tube is of stainless steel; its inside diameter is 2.50 cm. The lengths of the driver and driven sections are 120 and 170 cm, respectively. Shock waves were generated by increasing the pressure of the He driver until a selected Mylar diaphragm broke. Typical pressures in the driver and driven sections were 55 psig and 400−600 Torr, respectively. Two piezo-electric pressure sensors were stationed 10.0 cm apart at the end of the driven section. Their summed signal was recorded and digitized through Biomation 8100 and Northern Tracor signal analyzer and then stored in an IBM AT computer. The accuracy of the measured time interval is ±1 μs, which corresponds to an ambiguity of ∼8 K in the reflected shock temperature. The temperature in the reflected shock region was estimated according to the computational procedure recommended by Gardiner et al.[11] for very dilute reaction mixtures and the shock tube code developed by Mitchell and Kee (Sandia National Laboratory).[12] Identical results were obtained with the above algorithms for the mixtures used in these experiments. The effective heating time was defined as the time elapsed from the beginning of the reflected shock wave to the point where the pressure signal was 80% of that in the reflected shock region. The storage tank, gas handling line, and the shock tube were maintained at ∼135 °C throughout the experiments. 1,3,3-Trinitroazetidine was obtained from the U.S. Army Armament Research, Development and Engineering Center, Picatinny Arsenal. The temperature-dependent vapor pressure[13] is, for the solid,

$$\log(p/\text{Torr}) = 8.0106 - 3295.3/T(\text{K})$$

$$Q(\text{vaporization}) = 15.1\ \text{kcal/mol}$$

$$p(300\ \text{K}) = 0.001\ \text{Torr}, \quad p(375\ \text{K}) = 0.167\ \text{Torr}$$

and, for the liquid,

$$\log(p/\text{Torr}) = 7.7375 - 2900.6/T(\text{K})$$

$$Q(\text{vaporization}) = 13.3\ \text{kcal/mol}$$

High-purity helium and argon were used as driving and carrier gases, respectively. Research grade CO, CO_2, NO, and O_2 gases were used for GC and FTIR calibration, all from Matheson. An H_2CO−Ar mixture for GC calibration was made with an H_2CO/water solution from Mallickrodt, and an HCN reference mixture was generated from NaCN and sulfuric acid (both from Fisher).

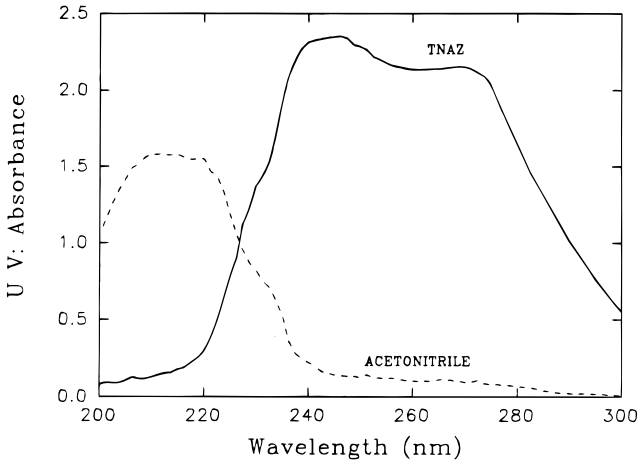

Figure 1. UV spectrum of 0.01 M TNAZ−acetonitrile solution (solid line, corrected for solvent absorption). The dashed line is the spectrum of the solvent. The thickness of the UV cell is 1 cm.

TNAZ−Ar mixtures were prepared as follows. A weighed amount of the solid was first introduced into a ∼6.5 L Pyrex flask that had been filled with Ar at room temperature [the vapor pressure of solid TNAZ is $\sim 9 \times 10^{-4}$ Torr]. The flask was pumped down quickly to $<10^{-3}$ Torr and then filled with Ar to ∼2 atm. The flask was then gradually heated to ∼135 °C and kept at that temperature for ∼16 h before use. Our stability tests on TNAZ indicated that in a Pyrex vessel premature decomposition does not occur; this mixture can be kept at 135 °C for several days without significant decomposition. However, decomposition was observed at $T > 190$ °C. In contrast, in a stainless steel tank, most of the TNAZ decomposed when kept at 110 °C for ∼12 h. Since the time spent from filling the driven section of the shock tube with the TNAZ−Ar mixture to initiating a shock wave is less than 30 s, we found no evidence of premature decomposition of TNAZ in the stainless steel shock tube.

Several analytical protocols had to be developed to monitor the loss of TNAZ and the appearance of NO_2 in real time and to analyze the reaction product distribution after ∼1.5 ms residence time under reflected shock conditions.

Spectrophotometric Method. The UV−visible absorption spectra of TNAZ in acetone or acetonitrile solution were recorded with a HP 8451A diode array UV−visible spectrophotometer. The spectra were taken at room temperature of a ∼0.01 M solution. A typical absorption spectrum is shown in Figure 1. TNAZ absorbs UV light strongly over the range 230−275 nm. The extinction coefficient of NO_2 at elevated temperatures was determined by Huffman and Davidson,[14] as shown in Figure 2. For real time measurements in these shock tube experiments, the technique employed in our previous study of nitromethane[15] proved unsatisfactory. Because of the rapid disappearance of the dioxide due to fast secondary reactions, only a thin layer (less than 0.5 cm in the case of nitromethane) of the gaseous product mixture, immediately behind the front of the reflected shock wave, contains detectable amounts of NO_2. Therefore it proved impractical to measure NO_2 by directing the light axially through the tube. Preliminary measurements at 290 nm, using an incident beam along the tube axis, did yield useful data on the *absorption coefficient* of TNAZ at elevated temperatures. The extinction coefficient increases substantially with rising temperature from $\epsilon = 75$ at 550 K to $\epsilon = 140$ at

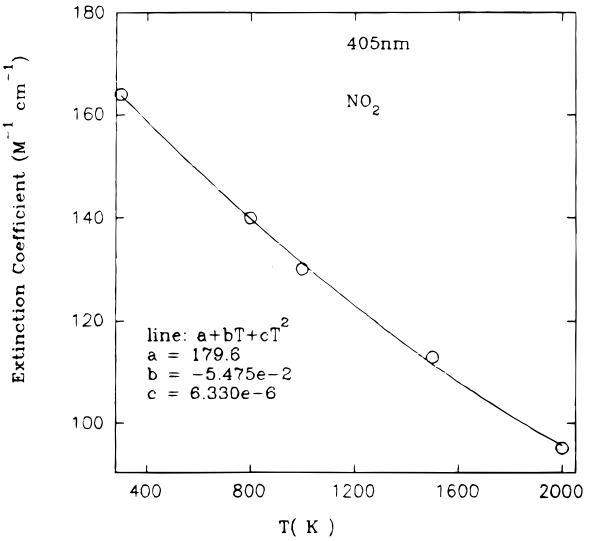

Figure 2. Temperature dependence of the extinction coefficients of NO_2 at 405 nm.

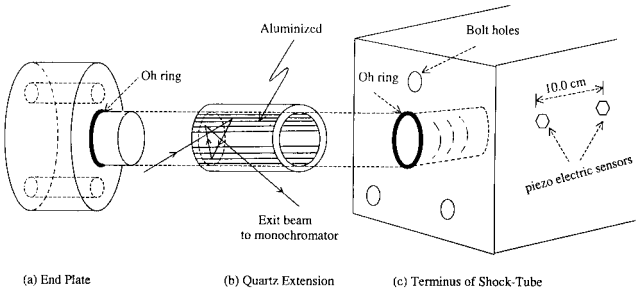

Figure 3. Schematic of the quartz extension of the shock tube. Sections of the quartz tube are aluminized to allow the entrance beam to reflect several times before it exits thus increasing the effective path of the beam in the small diameter shock tube. [The retaining Al girdle around the quartz tube is not shown.]

750 K, followed by a much smaller increase for $T > 750$ K. However, axial illumination was inadequate for obtaining rate data. To direct the optical path *normal* to the axis of the heated shock tube (2.5 cm inner diameter) and to develop a measurable UV absorption signal from TNAZ (at 271 nm) and NO_2 (at 405 nm), we increased the effective optical path length *normal* to the tube by attaching to it a quartz cylinder extension (2.50 cm i.d., 2 cm long). The outer wall of this tube was partially aluminized as indicated in Figure 3. With this configuration, more than 70% the probe beam makes more than three passes through the sample, while the rest of the beam is transmitted via a single pass. Thus a considerably higher level of attenuation by the gas sample was achieved. The width of the probe beam that illuminates the sample is about 8 mm, hence $I(t)/I_o$ measures the density of TNAZ or NO_2 that had been processed at the reflected shock temperature, averaged over a time interval of $\Delta t = 18\ \mu$s. The effective path length of the probe light through the sample was calibrated by filling the tube with a known concentration of diacetyl and measuring its absorption at 310 nm, where its extinction coefficient is 15. The effective path length was found to be 16 cm. The small change in residence time due to this extension was taken into account in analyzing the experimental results.

FTIR Spectroscopic Method. An electronically stabilized Polaris FTIR spectrometer from Mattson Instrumental Inc. was used for analyzing the distribution of reaction products as well as for recording IR spectrum of TNAZ in the gas phase.[16] Integrated peak areas were used to determine quantitatively the

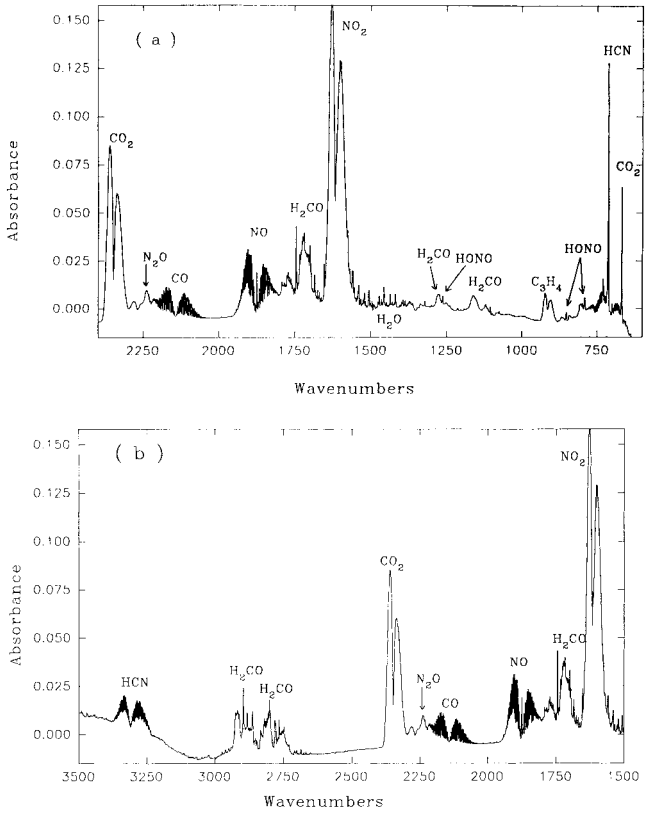

Figure 4. Typical IR spectrum of the product mixture in a shock tube pyrolysis experiments. Band assignments are indicated in the figure.

concentrations of HCN, CO, NO, and NO_2. Beer's law was found valid for all species over the concentration range we encountered in this work. A typical spectrum of the gas-phase product mixture is shown in Figure 4.

Gas Chromatographic Method. A Nicolet/IBM 9630 gas chromatograph with flame ionization detector and a HP 18790 chromatograph with a thermal conductivity detector were used to quantitatively determine the concentrations of the unreacted TNAZ and the reaction products, respectively. Immediately after each shock, a 16 mL sample at a measured pressure was collected through the sampling valve at the end of the driven section of the shock tube. A small portion of this sample was then injected into a 30 ft $\times$ $^1/_8$ in. stainless steel Hayesep DB 100/120 column through a six-port injection valve for analysis. The flow rate of carrier gas He is typically 25 mL/min. The column temperature was held at 25 °C for the first 5 min and then ramped at a rate of 6 °C/min until it reached the final temperature, 160 °C. The major reaction products CO_2, H_2CO, and HCN were well separated and quantitatively determined. Retention times of these compounds are 20, 34, and 38 min, respectively, under these conditions.

Due to the low vapor pressure of TNAZ we found that it was not possible to transfer the hot gas sample from the shock tube into the GC column without losing some of it during the transferring process due to condensation on cool spots. For this analysis the shocked gas mixture was extracted through the sampling valve into a 150 mL Pyrex flask, which was kept at 130 °C. The collected sample was then cooled to room temperature so that the TNAZ in the sample deposited on the walls of the container. Then 2 mL of acetonitrile or acetone was injected into the flask. The TNAZ was dissolved by swishing the solvent over the inner surface of the flask. Finally, 10 μL of this solution was injected into the GC with a column of 10% DC550, on Chromosorb, PAW-DMCS GC from Alltech.

TABLE 1: Calculated Equilibrium Concentrations for a Mixture of 0.074% TNAZ−Ar at 4 atm[a]

	T_{final} (K)			
	746[b]	996[c]	1197[d]	experiment[e]
TNAZ	0.0	0.0	0.0	
H_2	1.47×10^{-3}	1.47×10^{-3}	1.47×10^{-3}	
O_2	4.48×10^{-13}	9.38×10^{-10}	4.21×10^{-8}	
H_2CO	3.83×10^{-21}	6.45×10^{-18}	2.58×10^{-16}	0.10
CO	9.45×10^{-13}	1.96×10^{-9}	8.79×10^{-8}	0.40
CO_2	2.21×10^{-3}	2.21×10^{-3}	2.21×10^{-3}	0.14
CH_3CCH	0.0	0.0	0.0	trace
N_2	1.47×10^{-3}	1.47×10^{-3}	1.47×10^{-3}	
NO	4.71×10^{-14}	8.72×10^{-11}	3.71×10^{-9}	1.6
NO_2	8.00×10^{-20}	6.44×10^{-16}	5.71×10^{-14}	0.26
N_2O	4.86×10^{-19}	6.23×10^{-16}	2.26×10^{-14}	trace
HCN	3.36×10^{-29}	3.08×10^{-23}	2.93×10^{-20}	0.40
HONO	8.62×10^{-16}	7.05×10^{-14}	6.35×10^{-13}	trace

[a] The calculated equilibrium concentration (with constant enthalpy and pressure constraints) is in the unit of mole fraction. [b] Initial temperature was 700 K. [c] Initial temperature was 950 K. [d] Initial temperature was 1150 K. [e] Measured: $[\text{species}]_{t=2ms}/[\text{TNAZ}]_{t=o}$ under shock conditions at 950 K.

Temperatures of the injector, the column, and the FID detector were all kept at 150 °C. The flow rate of the He carrier gas was ∼25 mL/min. The retention time for TNAZ is ∼8.5 min. No significant decomposition of authentic samples was detected under these conditions. However, the analytical results from the shocked samples were highly scattered. The chromatograms of all the experiments were recorded with a Hewlett-Packard 3396A Integrator.

Results

A. Gas-Phase IR Spectra of TNAZ. The structure of TNAZ in the solid state was determined by Archibad et al. by X-ray crystallography.[17] IR spectra in solution[18] and of the solid[8] have been recorded, and assignments of the absorption frequencies were attempted. Recently, Thompson et al.[19] recorded the IR spectra of matrix-isolated TNAZ and of istopically labeled TNAZ. Twenty-four of the 45 fundamental frequencies were assigned in that investigation. We recorded the gas-phase IR spectrum of TNAZ using a heated Teflon IR cell (at 107 °C). The experimentally observed frequencies and their assignments are reported in ref 16. The IR spectra of the solid-phase and matrix-isolated TNAZ in Ar at 15 K are almost (but not entirely) identical. With a reported value of $\Delta H_f°$ for TNAZ (ab initio calculations[20]), our gas-phase vibrational frequencies, and structural parameters of the molecule, the thermodynamic parameters $\Delta H°$, $S°$, C_p, etc. as functions of temperature were calculated, using standard statistical thermodynamics relations. The computed thermochemical values for TNAZ were least-squares fitted to the standard NASA seven-parameter polynomials. It was then possible to estimate whether for TNAZ pyrolysis, over the temperature range 950−1500 K, the observed product distributions approach their equilibrium levels (i.e., minimum total free energy for the entire sample). Inspection of Table 1 clearly showed that our measured product distribution as well as those reported for pyrolyses of the solid and of various solutions were kinetically limited.

B. Kinetics of TNAZ and NO_2 in Reflected Shock Wave. The loss of TNAZ and the production of NO_2 under reflected shock conditions were monitored at 271 and 405 nm, respectively. A typical kinetic curve is shown in Figure 5. The initial rise in absorbance (TNAZ) is due to the sudden jump in the temperature and the pressure of the reaction mixture in the tube. The two stages in this rise are due to the incident and the reflected shock, respectively. As can been seen in Figure 5b, the disappearance of TNAZ is first order, indicating a unimolecular process. At ∼780 K the reaction is complete over the time interval of ∼1.5 ms. An Arrhenius plot of k_{uni} so obtained is shown in Figure 6. The unimolecular rate constant can be expressed as

$$k_{uni} = 10^{13.96\pm0.63} \exp[(-39.54 \pm 2.36)/RT], \text{ s}^{-1}; \quad E_a \text{ in kcal/mol} \quad (1)$$

The total pressures in these experiments ranged from 3 to 5 atm, of which the TNAZ is 0.16%, and no pressure dependence

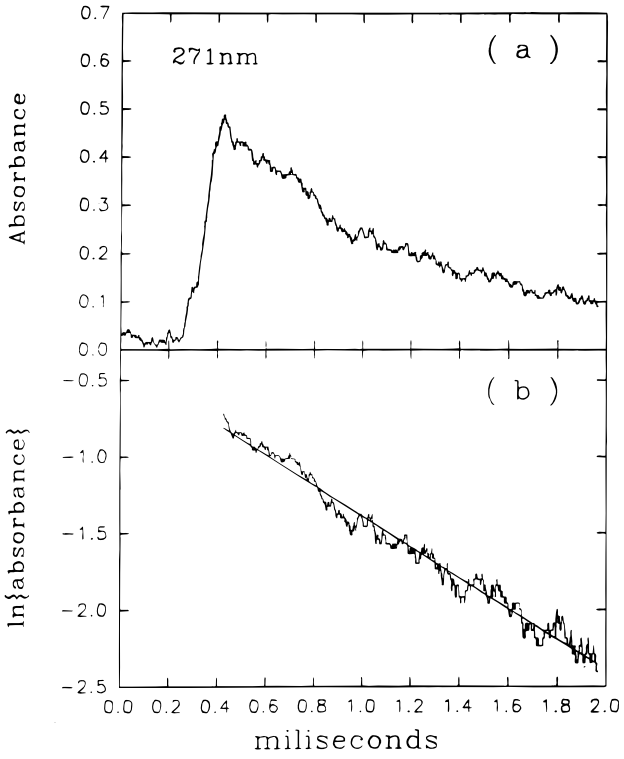

Figure 5. Typical absorbance vs time curve at 271 nm due to TNAZ. Solid line in (b) is the least-squares fit to the experimental data. Conditions: $[\text{TNAZ}]_o = 0.158\%$ (mole fraction percentage), $T = 779$ K, $P = 3.49$ atm.

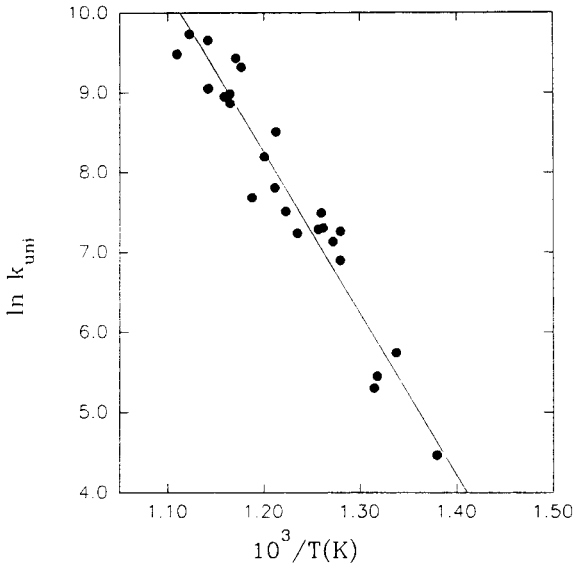

Figure 6. Unimolecular rate constant observed. $[\text{TNAZ}]_o = 0.158\%$ (mole fraction percentage), $P = 3.0-5.0$ atm. Symbols are experimental data, and the solid line is the least-squares fit of the data.

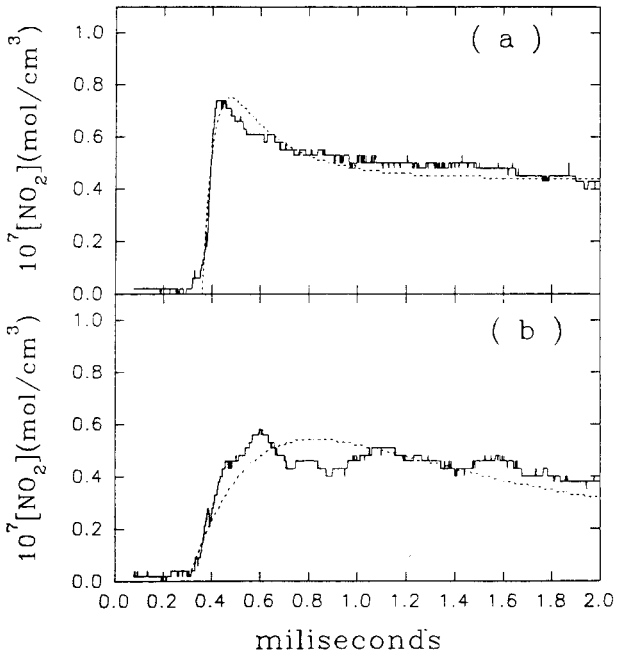

Figure 7. Typical absorbance vs time curves at 405 nm due to NO_2. Dashed lines are from simulations with reactions R2−R4 and rate constants in Figure 8. Conditions: (a) $T = 903$ K; $P = 4.67$ atm.; $[TNAZ]_o = 9.95 \times 10^{-8}$ mol/cm^3. (b) $T = 802$ K; $P = 3.84$ atm.; $[TNAZ]_o = 9.21 \times 10^{-8}$ mol/cm^3.

in k_{uni} was found, indicating that k_{uni} in eq 1 is at the high-pressure limit.

The residual TNAZ was also measured in (expansion wave) quenched samples with GC, as described in the Experimental Section. The temperature range that can be investigated via this method was limited to 625−770 K since only over this range do detectable amounts of unreacted TNAZ persist after ~1.5 ms. Values of k_{uni} so derived were highly scattered and appeared to be too large, indicating that there was additional loss of TNAZ during the complicated sample-handling process.

The production of NO_2 during the pyrolysis of TNAZ in the reflected shock waves was measured by means of its UV absorption at 405 nm. Typical response curves for NO_2 are shown in Figure 7. At high temperatures, there is an initial sharp rise in NO_2 concentration, which is followed by a short rapid decrease, and then $[NO_2]$ remains nearly constant. At low temperatures, a relatively slow increase was followed by a slow decrease: refer to Table 2 where all the features for the experimentally obtained $[NO_2]$ kinetic curves are summarized; $[NO_2]_{max}$ and $[NO_2]_f$ indicate the peak and final values of $[NO_2]$ in each curve. Since a full mechanism for the overall reaction is complicated, a preliminary initial scheme was developed to simulate *these* kinetic results for NO_2

$$\text{TNAZ} \xrightarrow{k_2} \text{X} + \text{NO}_2 \qquad \text{(R2)}$$

$$\text{X} + \text{NO}_2 \xrightarrow{k_3} \text{products(1)} \qquad \text{(R3)}$$

$$\text{X} + \text{fragments} \xrightarrow{k_4} \text{products(2)} \qquad \text{(R4)}$$

where X represents one or more intermediates (free radicals) in the overall reaction. Each reaction in the above model represents many elementary steps (explicitly cited in the final mechanism). Reaction R4 was assumed to be pseudo first order in these simulations.

TABLE 2: NO_2 Formation in Shock-Heated TNAZ−Ar Mixture[a]

expt	T_5 (K)	P_5 (atm)	$[TNAZ]_5$ (mol/cm^3)	$[NO_2]_{max}$ (mol/cm^3)	$[NO_2]_f/[TNAZ]_5$
456	780	3.62	8.94×10^{-8}	5.0×10^{-8}	0.45
457	765	3.54	8.71×10^{-8}	3.2×10^{-8}	0.23
459	765	3.57	8.99×10^{-8}	4.1e10^{-8}	0.33
461	780	3.77	9.28×10^{-8}	4.4×10^{-8}	0.43
462	825	3.58	8.35×10^{-8}	3.0×10^{-8}	0.24
465	903	4.67	9.95×10^{-8}	7.4×10^{-8}	0.40
466	802	3.84	9.21×10^{-8}	6.1×10^{-8}	0.43
467	766	3.78	9.5×10^{-8}	7.1×10^{-8}	0.42
469	859	5.05	1.13×10^{-7}	7.2×10^{-8}	0.34
470	740	5.01	9.0×10^{-8}	6.2×10^{-8}	0.30
471	991	4.83	9.37×10^{-8}	5.4×10^{-8}	0.33
472	1095	4.41	7.7×10^{-8}	5.8×10^{-8}	0.2
476	842	4.13	9.45×10^{-8}	1.1×10^{-7}	0.30
477	780	3.62	8.94×10^{-8}	3.9×10^{-8}	0.28
478	766	3.60	9.06×10^{-8}	5.0×10^{-8}	0.44

[a] Quantities with subscript 5 represent the values in the reflected shock region. $[TNAZ]_5$ is the concentration of TNAZ before reaction.

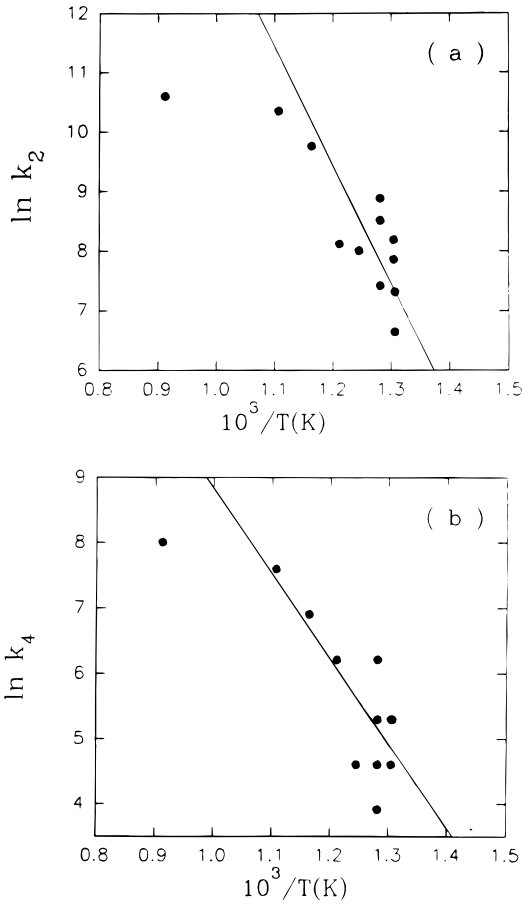

Figure 8. Rate constants for reactions R2 and R4 used in simulating the experimentally observed $[NO_2]$ vs time kinetic curves shown in Figure 7.

The differential equations for steps R2−R4 were integrated numerically with k_2, k_3, and k_4 as adjustable parameters to best fit the observed levels of NO_2. Nearly quantitative agreements with the experimental records were achieved in these calculations. Typical calculated kinetic curves are shown as the dotted lines in Figure 7. Temperature dependencies of the rate constants derived from the simulations are plotted in Figure 8. As drawn, the solid line in Figure 8a is three times the values of k_{uni} in eq 1. However, there is significant scatter of the experimental points. Nonetheless, the reasonably good fit of

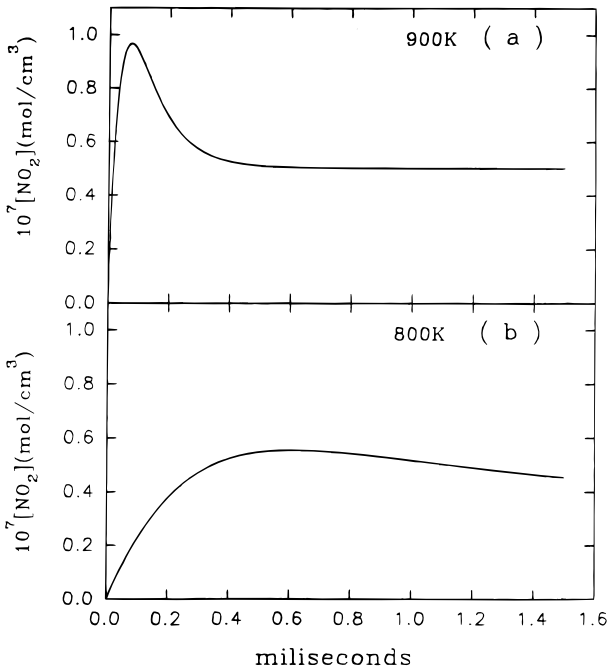

Figure 9. Time-dependent production levels of NO_2 computed per the full mechanism (Table 4). Conditions: $[TNAZ]_o = 9.0 \times 10^{-8}$ mol/cm^3, $[Ar]_o = 5.42 \times 10^{-5}$ mol/cm^3.

this line to the rate constant for R2 suggests that the three NO_2 groups dissociate successively from the molecule during the initial stages of pyrolysis. Successive fission of the two NO_2 groups in TNAZ has been reported previously by Anex et al.[21] They investigated the multiphoton dissociation of TNAZ in the IR under collisionless conditions (molecular beams) but did not determine rates. k_3 values span a range from 6×10^7 to 1×10^8 without an apparent temperature dependence. This is consistent with the fact that most bimolecular *free radical* reactions have very low activation energies and hence are insensitive to temperature over the range covered in these experiments. The rate constant k_4 increases with temperature with an activation energy of ~26 kcal/mol (Figure 8b). Clearly, the above scheme needs to be expanded, and additional intermediate species should be included in the mechanism (see below).

C. Reaction Products. Major products from high-temperature pyrolysis of TNAZ are NO, NO_2, CO, CO_2, HCN, and H_2CO; $H_3C-C\equiv CH$ is a minor product. A typical infrared spectrum of the shock-heated reaction mixture is shown in Figure 4. The assignments of the absorption bands are indicated. The existence of HONO has been positively identified, but quantitative measurements of its concentration through both FTIR and GC were difficult due to its very low levels. The characteristic doublet at 926 cm^{-1} was assigned to C_3H_4, and the broad absorption band at around 2900 cm^{-1} is an overlap of H_2CO and a small amount of unreacted TNAZ. The rather weak band at about 2250 cm^{-1} is tentatively assigned to N_2O, and its existence in the product mixture needs to be further explored; N_2O was not observed when TNAZ was pyrolyzed in the solid phase. N_2O_2, N_2O_3, and HNO were not found in the shock-heated samples.

The temperature dependencies of the product distributions are shown in Figures 9−11. Magnitudes for HCN, NO, CO and NO_2 were obtained from FTIR band areas, while those for CO_2 and H_2CO were determined via GC. The large scatter in the values for [NO] is due to the uncertainty of the peak areas of the NO absorption band, which is overlapped with traces of

SCHEME 1

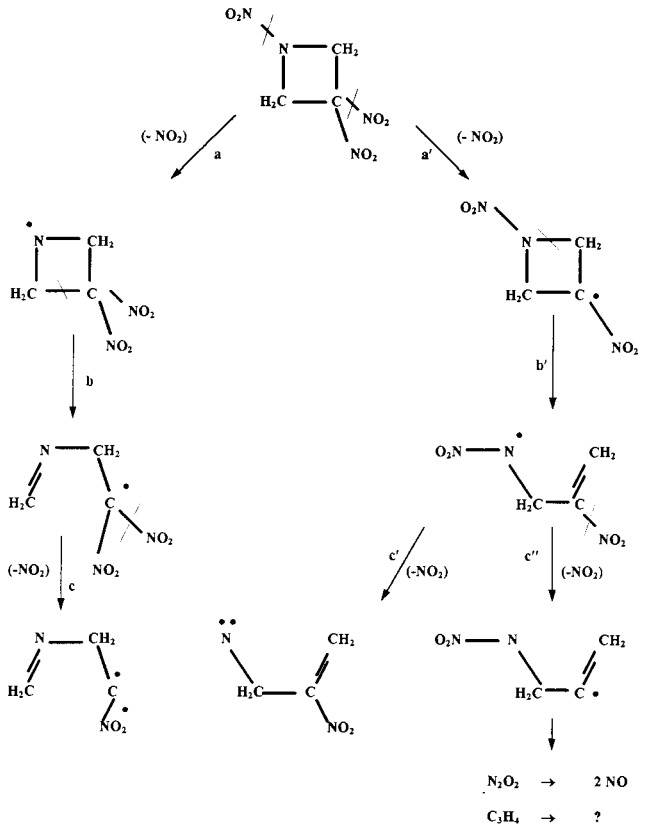

water present in the chamber of the FTIR instrument. [NO] and $[CO_2]$ are nearly constant over the entire temperature range. [CO] increases slowly and $[NO_2]$ decreases slowly with temperature. A large decrease in $[CH_2O]$ with temperature was observed. It is well-known that CH_2O decomposes to CO and H_2 over this temperature range. Clearly, the reactions leading to the changes in [CO] and $[NO_2]$ are more complicated. Notice that the $[NO_2]_f$ listed in Table 2 agrees fairly well with the values of $[NO_2]$ in Figure 11a, indicating that no further reactions take place in the quenched mixture after extraction from the shock tube.

Discussion

A sequence of degradation steps that accounts for the experimental observations reported in the proceeding section should provide a rationale for the product distributions and their rates of production, consistent with available estimates of the thermochemical and kinetic constraints. It is evident that there are gaps in the totality of available data both in the time domain (UV absorption vs analysis of quenched mixtures) and composition domain (no information on radical intermediates). A benchmark magnitude for a unimolecular fission of a $C-NO_2$ bond is that reported for nitromethane.[22,15]

$$k^{\infty}_{uni} = 1.78 \times 10^{16} \exp(-29440/T),\ s^{-1} \qquad (2)$$

Anex, Allman, and Lee[21] induced the decomposition of TNAZ with multiphoton infrared excitation in a molecular beam. Successive fissions of two NO_2 groups in the molecule were observed, and the determined products (presumably under collisionless conditions) were C_3H_4 and N_2O_2. The absence of NO as an initial product suggests that gas-phase nitro−nitrite isomerization followed by NO loss is not a significant side reaction but that N_2O_2 subsequently dissociates to 2NO. Also

SCHEME 2[a]

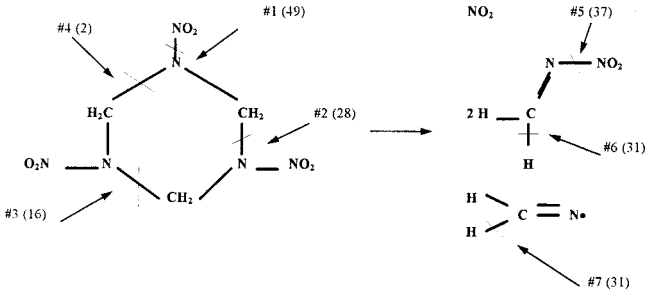

[a] —, #*n*, (ΔE): position, order, and bond breaking energy (kcal/mol).

SCHEME 3

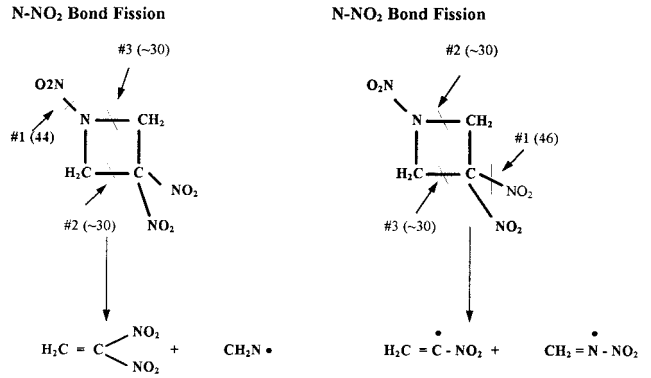

CH_2NNO_2 was not detected presumably because it may be produced late in the reaction pathways. The proposed reaction sequence is shown in Scheme 1. Since their experimental methods cannot identify the position of the NO_2 lost in each step, both the C−NO_2 and N−NO_2 fission routes were presented. A subsequent theoretical analysis by Politzer and Seminario[23] indicated that barrier heights for C−NO_2 and N−NO_2 are very close indeed, with values of 44.6 and 46.6 kcal/mol, respectively. The possible reason for the rather low activation energy for the C−NO_2 bond rupture is that the generated radical species is stabilized by delocalization of the unpaired electron by the adjacent NO_2 group. Calculations also indicated that the reaction energies for secondary losses of NO_2 as shown in Scheme 1 are energetically unfavorable. For example, the reaction energies for reaction c′ and c″ are 38.1 and 67.1 kcal/mol, respectively, whereas by forming the following two compounds the corresponding values are −22.1

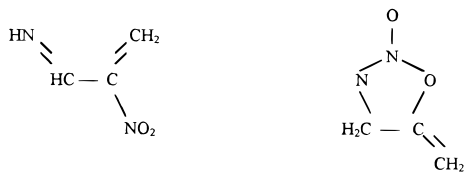

and −19.6 kcal/mol. However, activation energies for these steps have not been assessed.

Oyumi and Brill[24] studied the thermolysis of rapidly heated solid TNAZ and determined the evolution of products via FTIR spectroscopy. The major reaction products were NO, NO_2, HCN, H_2CO, CO, and HONO. NO_2 was rapidly produced at the onset of pyrolysis and then was consumed gradually during the reaction. This observation supports the idea that NO_2 fission is the first step. The relative quantities of reaction products they observed at the end of the reaction (∼10 s) are [NO] > [HCN] > [NO_2] ∼ [CO_2] ∼ [H_2CO] ∼ [CO] > [HONO]. N_2O was not present among their reaction products. This contrasts

SCHEME 4

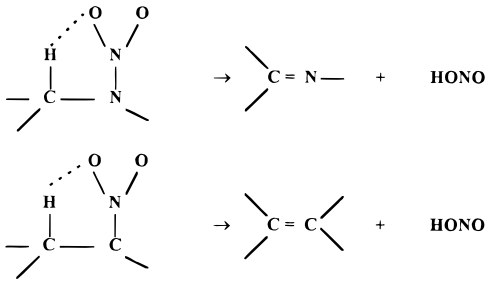

SCHEME 5

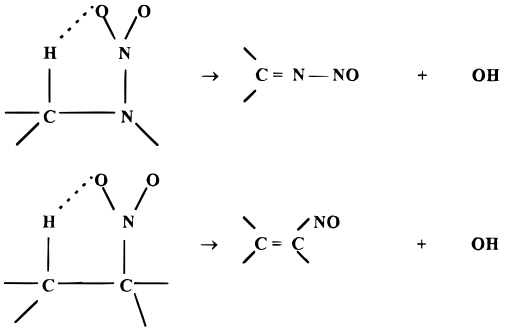

TABLE 3: Thermochemical Data of Chemical Species Involved in the Pyrolysis of TNAZ

species	$\Delta H°_{f\,298}$ (kcal mol^{-1})	$S°$ (cal K^{-1} mol^{-1})	ref
TNAZ	30.7	85.59	*a,b*
•N(NO2)(NO2) (TNAZr1)	66.1		*a*
O2N–N(•)–NO2 (TNAZr2)	68.8		*a*
CH_2N	59.11		*c*
CH_2=N−NO_2	33.64		*c*
NO_2	8.17	57.40	*d*
HCN	32.27	48.24	*d*
NO	21.81	50.37	*d*
CO	−26.42	47.24	*d*
CO_2	−94.05	51.10	*d*
HONO	−18.75	60.72	*d*
H	52.10	27.42	*d*
OH	9.40	43.91	*d*
H_2CO	−25.95	52.29	*d*
H_3C−C≡CH	44.32	59.34	*d*
HCO	10.04	53.62	*d*
N_2O	19.50	52.58	*d*
CN	104.47	48.43	*d*
HNO	24.39	52.80	*d*

[a] Politzer, P.; et al. *J. Mol. Struct. (THEOCHEM)* **1995**, *338*, 249. [b] Yu, C.-L.; Zhang, Y.-X.; Bauer, S. H. *J. Mol. Struct.* (*THEOCHEM*), in press. [c] Melius, C. F. In *Chemistry and Physics of Energetic Materials*; Bulusu, S. N., Ed.; Kluwer Academic Publisher: The Netherlands, 1990. [d] Burcat, A.; McBride, B. *Ideal Gas Thermodynamic Data for Combustion and Air-Pollution Use*; Technion: 1995.

sharply with results reported for most nitramines, wherein H_2CO and N_2O always appear together in the mixture of products. It is presumed that these are derived from the decomposition of CH_2NNO_2 formed earlier in the reaction. The presence of HONO in the mixture suggests that the five-center HONO elimination (see Scheme 4) as the initial step of the reaction may also occur in the TNAZ pyrolysis, although HONO could also be produced from secondary reactions.

The thermal decomposition of TNAZ and $DNAZ^+$ (3,3-

TABLE 4: TNAZ Pyrolysis Mechanism[a]

no.	reaction	*A*	*n*	E_a	ref
(1)	TNAZ → NO_2 + TNAZr1	4.56E13[b]	0	39.54	*c*
(2)	TNAZr1 → TNAZr3	1E16	0	25.0	*c*
(3)	TNAZr3 → CH2N + $CH2C(NO_2)_2$	1E16	0	30.0	*c*
(4)	TNAZ → NO_2 + TNAZr2	4.56E13	0	39.54	*c*
(5)	TNAZr2 → TNAZr4	1E16	0	25.0	*c*
(6)	TNAZr4 → CH_2CNO_2 + CH_2NNO_2	1E16	0	30.0	*c*
(7)	TNAZr4 → 2NO + TNAZr5	5E15	0	30.0	*c*
(8)	TNAZr5 → NO_2 + C3H4	1E15	0	30.0	*c*
(9)	$CH_2C(NO_2)_2$ → CH_2CNO_2 + NO_2	1E16	0	30.0	*c*
(10)	CH_2CNO_2 → CH_2O + CNO	1E16	0	20.0	*c*
(11)	CH_2NNO_2 → CH_2N + NO_2	1E16	0	25.0	*c*
(12)	CH_2N + M → HCN + H + M	1E16	0	30.0	*d*
(13)	CH_2O + M → H2 + CO + M	2.1E15	0	35.01	*e*
(14)	NO_2 + H → NO + OH	3.5E14	0	1.5	*d*
(15)	H + H + M → H_2 + M	1E18	−1	0	*d*
(16)	H + OH + M → H_2O + M	1.6E22	−2	0	*d*
(17)	CH_2O + H → H_2 + HCO	2.19E8	1.77	3.0	*d*
(18)	CH_2NNO_2 + H → HONO + CH_2N	1E12	0	5.0	*d*
(19)	HONO + H → NO_2 + H_2	1E12	0	1.0	*d*
(20)	HCN + OH → CN + H_2O	1.45E13	0	10.929	*n*
(21)	CNO + OH → NO + CO + H	1E13	0	0	*c*
(22)	CH_2O + OH → H_2O + HCO	5.12E15	0	9.916	*c*
(23)	HCO + OH → H_2O + CO	3.01E13	0	0	*g*
(24)	HONO + OH → NO_2 + H_2O	1.08E12	0	0	*f*
(25)	CH_2NNO_2 + (OH) → CH_2O + N_2O + (OH)	1E13	0	0	*d*
(26)	CH_2N + NO_2 → HONO + HCN	3E10	0	0	*c*
(27)	CO + NO_2 → CO_2 + NO	1.26E14	0	27.6	*d*
(28)	CH_2NNO_2 + (H_2O) → CH_2O + N_2O + (H_2O)	1E11	0	2.0	*d*
(29)	CNO + NO_2 → NO + NO + CO	5E9	0	0	*c*
(30)	CO + OH → CO_2 + H	1.51E7	1.3	−0.758	*d*
(31)	CN + N_2O → N_2 + NCO	1E13	0	0	*d*
(32)	CNO + H → HCNO	1E14	0	0	*c*
(33)	OH + HCNO → HNO + HCO	1E13	0	5.0	*d*
(34)	OH + HNO → H_2O + NO	7.68E16	0	9.916	*d*
(35)	CNO + NO → CO_2 + N_2	1E10	0	0	*c*
(36)	CNO + H_2O → HNO + HCO	3E11	0	0	*c*
(37)	HCO + M → CO + H + M	2.5E14	0	16.8	*d*
(48)	CO + H + M → HCO + M	6.31E20	−1.82	3.688	*g*
(39)	H + HCO → H_2 + CO	3.31E14	0	0	*l*
(40)	H + HNO → H_2 + NO	7.83E13	0	0	*k*
(41)	H + HCN → CH_2N	3.31E13	0	4.844	*h*
(42)	CN + HCN → H + C_2N_2	3.8E7	1.57	0.0994	*i*
(43)	HCO + HCO → $(CHO)_2$	3.01E13	0	0	*m*
(44)	HCO + NO2 → H + NO + CO_2	8.39E15	−0.75	1.929	*j*
(45)	HCO + NO2 → HONO + CO	1.239E23	−3.29	2.355	*j*
(46)	CH_2N + H → CH_2NH	7.68E16	0	9.916	*c*

[a] Rate expression in the mechanism is in the form of $AT^n \exp(-E_a/RT)$. The unit of rate constant is $[\text{mol/cm}^3]^{-(m-1)}\ \text{s}^{-1}$, where *m* is the order of the reaction. [b] Read as 4.56×10^{13}. [c] This work. [d] Melius, C. F. In *Chemistry and Physics of Energetic Materials*; Bulusu, S. N., Ed.; Kluwer Academic Publishers: Boston, 1990. [e] Miyauchi, T.; Mori, Y.; Imamura, A. *Symp. (Int.) Combust.* **1977**, *16*, 4073. [f] Cox, R. A. *J. Photochem.* **1974**, *3*, 175. [g] Tsang, W.; Hampson, R. F. *J. Phys. Chem. Ref. Data* **1986**, *15*, 1087. [h] Tsang, W.; Herron, J. T. *J. Phys. Chem. Ref. Data* **1991**, *20*, 609. [i] Zabarnick, S.; Lin, M. C. *Chem. Phys.* **1989**, *134*, 185. [j] Lin, C.-Y.; Wang, H.-T.; Lin, M. C.; Melius, C. F. *Int. J. Chem. Kinet*. **1990**, *22*, 455. [k] Podonov, A. F.; et al. *Kinet. Catal.* **1981**, *22*, 689. [l] Reilly, J. P.; et al. *J. Chem. Phys*. **1978**, *69*, 4381. [m] Steockel, F.; et al. *Chem. Phys.* **1985**, *95*, 135. [n] Szekely, A.; Hanson, R. K.; Bowman, C. T. *Int. J. Chem. Kinet.* **1984**, *16*, 1609.

dinitroazetidium ion) was investigated in solution with several solvents and in the solid phase by Oxley et al.[25a] over the temperature range 160−280 °C. They reported the following first-order rate constants: $3.55 \times 10^{17} \exp(-46.6/RT)$ for the solid phase, $5.61 \times 10^{14} \exp(-40.3/RT)$ for solution in benzene, $2.89 \times 10^{16} \exp(-43.6/RT)$ for solution in acetone, and $2.62 \times 10^{11} \exp(-30.7/RT)$ for solution in methanol. Clearly, the nature of the solvent strongly affected the kinetics of reaction. They observed the gaseous products N_2, NO, CO, CO_2, and a trace of N_2O. However, NO_2 was not detected with their analytical technique. Several organic compounds were also generated: 3,5-dinitropyridine, 1-formyl-3,3-dinitroazetidine, 1,3-dinitroazetidine, 1-nitroso-3,3-dinitroazetidine, and 1-nitroso-3-nitroazetidine. The amounts of these compounds were not determined. It should be noted that none of these compounds has been observed as a reaction product in the gas-phase shock tube pyrolysis of TNAZ.

Garland and Nelson[25b] recently reported on product distributions generated by irradiating solid TNAZ with 248 nm laser light. The effluent gaseous products were ionized by pulses of 118 nm radiation and analyzed mass spectrometrically in a time-of-flight instrument. They concluded that there occurred an initial unimolecular nitro−nitrite rearrangement (presumably in the solid phase), which was followed by loss of NO, and subsequently a bimolecular reaction generated nitrosodinitroazetidine. While NO_2 production did occur early, it was not due to an initial decomposition step.

Melius[26] performed a series of theoretical calculations on decomposition mechanisms of several energetic materials, in particular RDX (hexahydro-1,3,5-trinitro-s-triazine) and HMX

(1,3,5,7-tetranitro-1,3,5,7-tetraazacyclooctane), based on the BAC-MP4 program. Thus he estimated thermochemical magnitudes for the stable and radical species generated in these reactions. Bond dissociation energies and activation energies of all possible steps in the decomposition process were obtained. These indicated that fission of the $N-NO_2$ bond was the first step in the decomposition and that the following steps involved breaking the second nearest bond to the radical center, yielding CH_2N and CH_2NNO_2 in the case of RDX (see Scheme 2). A hydrogen atom is then released from CH_2N to initiate a series of reactions among small molecular weight species of radicals and molecules that eventually lead to the final mixture of products. A mechanism consisting of 258 elementary steps was proposed to model the RDX flame. Wu and Fried[27] proposed a mechanism for the decomposition of RDX based on ab initio analysis and concluded that the activation energy for $N-NO_2$ bond rupture was 34.2 kcal/mol whereas that for a concerted ring fission (to three methylene nitramines) was 52.5 kcal/mol.

On applying the bond-breaking pattern of RDX to TNAZ, one may write the sequence of reactions for both $N-NO_2$ and $C-NO_2$ bond ruptures shown in Scheme 3. Although no kinetic data on the decomposition of $CH_2C(NO_2)_2$ is available, it is plausible that over the temperature range 750−1100 K it rapidly decomposes via C−N bond rupture. Attempts to prepare $CH_2C(NO_2)_2$ as a potential explosive did not succeed because of its tendency to decompose at low temperatures.[28] The most plausible decomposition reaction of the generated radical $CH_2\dot{C}NO_2$ would be:

$$CH_2\dot{C}NO_2 \rightarrow CH_2O + \dot{C}NO \qquad \text{(R5)}$$

There are other possibilities for reactions that are not indicated in Scheme 3. These are not dominant in the decomposition of TNAZ, but they contribute to the overall fragmentation process. One may imagine a five-center HONO elimination reaction as an initial step in the decomposition of nitramines and nitrocompounds (Scheme 4). The presence of HONO among the reaction products is often used as evidence for such a process, but as we pointed out earlier, HONO can be formed from secondary reactions. Examples of HONO elimination as a first step of decomposition of nitro compounds (such as nitroethane) do exist, and energy barriers for such processes are normally less than those for the corresponding NO_2 bond fission steps, but the rate may be low due to low preexponential factors that are typical for such reactions. BAC-MP4 calculations indicate that NO_2 formation is more likely to occur than direct HONO elimination for N−nitro compounds whereas the opposite is true for C−nitro compounds.

Concerted decomposition of RDX was observed by Zhao, Hintsa, and Lee[29] who used multiphoton excitation of the compound in a molecular beam. A similar process was reported by Kamo et al. [10] and in our report[9] on the thermal decomposition of azetidine (see R1). The rate constant quoted is at the high-pressure limit for the temperature range 800−1100 K. A corresponding concerted decomposition of TNAZ (R6) would

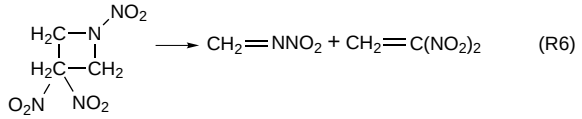

(R6)

have a relatively high activation energy, and is not likely to contribute to the pyrolysis.

Experimental data for the thermal decomposition of dimethylnitramine by Golden et al.[30] suggest that under their conditions

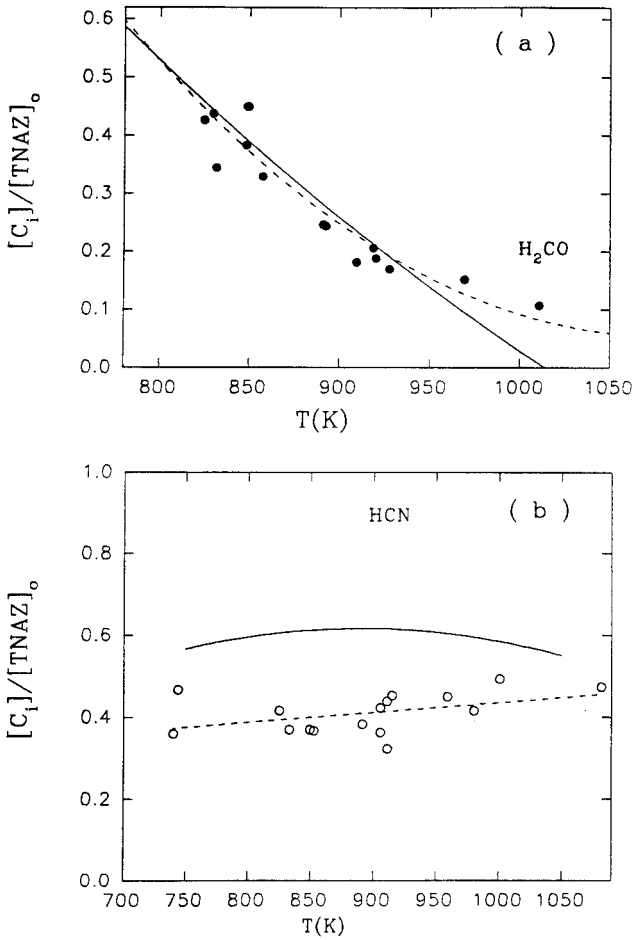

Figure 10. (a) Measured ratios (●) of $[H_2CO]/[TNAZ]_o$ in quenched samples for a range of reflected shock temperatures. The dashed line is a visual trend of the data for comparison with the computed (solid line) ratios per the full mechanism (Table 4). (b) Same as part a, for HCN. Initial concentrations of TNAZ and Ar in the calculations are as in Figure 9.

TNAZ might undergo a nitro−nitrite isomerization process prior to decomposition. The reported activation energy for isomerization is much less than that of NO_2 bond fission. However, the quantum chemical calculation by Grodzicki et al.[31] on two four-member ring nitramine compounds (1,2-diazacyclobutane and its 1,3-dinitramine derivative) predicted an activation energy of 140 kcal/mol for isomerization. It seems that for such compounds (including TNAZ) decomposition through nitro−nitrite arrangement is not a favorable route.

Another possible step is the formation of OH radical by migration of a neighboring H atom onto the O atom on adjacent NO_2 (Scheme 5). Subsequent decompositions of the generated radicals will give NO and then HCN and $CH_2{=}C(NO_2)_2$, which lead to the observed products H_2CO, CO, and CO_2 upon oxidation. The activation energy for the reaction in Scheme 5, however, is difficult to estimate. The bond dissociation energy for this C−H bond fission was estimated to be 94 kcal/mol by Melius.[26]

Available thermochemical parameters for the 19 species generated in the decomposition of TNAZ are complied in Table 3. An overall mechanism for this pyrolysis (Table 4) was developed on the basis of considerations presented in the preceding discussion. This is a minimal set of reactions (along with their temperature-dependent rate constants) that upon integration reproduce both the time-dependent absorption data (UV) and the product distributions found in the quenched

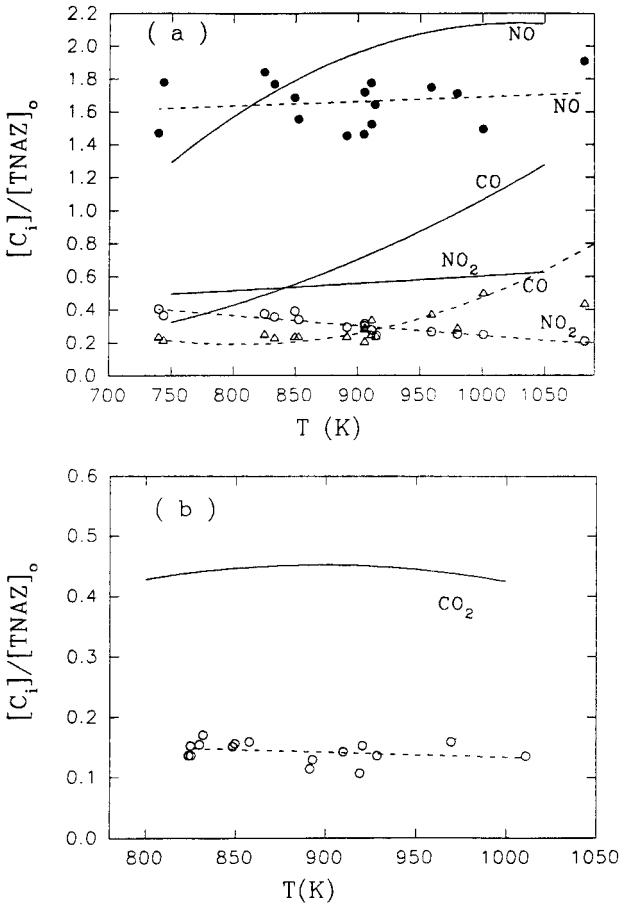

Figure 11. (a) Points indicate the measured ratios (dashed line are visual correlations) compared with the calculated trends for NO, CO, and NO_2. (b) Same as part a, for CO_2. Initial concentrations of TNAZ and Ar in the calculations are as in Figure 9.

samples, for a range of reflected shock temperatures, over the interval 825−1000 K. No doubt, due to the complexity of this system many more reactions between the smaller species concurrently participate in the overall conversion, as suggested by the 258 steps proposed by Melius[26] for RDX. At this stage we have no evidence that incorporating the additional steps will improve the fit of the computed product distributions to those observed. However, we surmise that shock tube pyrolysis studies of mono- and dinitroazetidines, similar to this investigation of the trinitro species, will provide additional constraints on the fragmentation routes for this family of substituted four-member rings.

In Table 4 the following molecule and radical intermediates play significant roles during the early stages of pyrolysis:

TNAZ

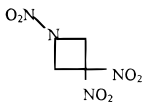

TNAZr1

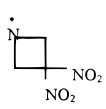

TNAZr2

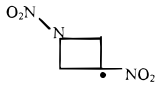

TNAZr3

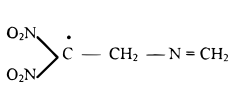

TNAZr4

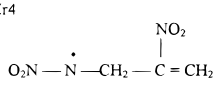

TNAZr5

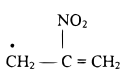

Note that theoretical calculations by Politzer et al.[23] indicated that the N−NO_2 and C−NO_2 bond dissociation energies are about equal. We took this into account by allowing half of the TNAZ dissociation to proceed via N−NO_2 and half via C−NO_2 fission. Also, their calculations suggested that the ring opening and the subsequent dissociations [(2),(3), (5)−(8] were very fast reactions. Rate constants for these reactions in Table 4 are estimated values, but they can be lowered or raised significantly without affecting the outcome of the overall concentrations as long as they do not become rate limiting.

C_3H_4 was found by Anex et al.[21] and in our samples as one of the reaction products. The most plausible route for its formation is through the parallel dissociation of TNAZr4 via (6) and (7). The branching ratio was chosen to be 0.5 in favor of (6) to best fit our experimental results. C_3H_4 follows from (7) and (8). In Table 4, the rate constants for the various steps were abstracted either from the literature or derived from analogous chemical reactions.

Finally, we present several graphs that illustrate the levels of agreement achieved between the analytical data and the calculated concentrations. The time-dependent production of NO_2 shown in Figure 9 (per the mechanism in Table 4) should be compared with that in Figure 7. Note that the origin for the onset in Figure 7 was plotted at $t = 0.3$ ms. Figure 10a,b shows acceptable agreement of magnitude and trends with temperature for H_2CO and HCN. From Figure 11a it is evident that the analytical data for NO, derived from its narrow line FTIR spectrum, is highly scattered. The mechanism calls for a slight increase with rising temperature for NO_2 and a larger one for NO. This we attribute to difficulties with the analytical protocol for products generated in this complex mixture at the level of 750 ppm of TNAZ.

In conclusion we present Table 4 as a viable mechanism for the pyrolysis of TNAZ in the gas phase, under high Ar dilution, for temperatures up to 1000 K, that merits further study.

Acknowledgment. We gratefully acknowledge the financial support from Army Research Office under Grant No. DAAH04-95-1-0130 for this investigation.

References and Notes

(1) Alexander, M. H.; Dagdigian, P. J.; Jacox, M. E.; Kolb, C. E.; Melius, C. F.; Rabitz, H.; Smooke, M. D.; Tsang, W. *Prog. Energy Combust. Sci.* **1991**, *17*, 263−296 (a review).

(2) Bulusu, S. N., Ed. In *The Chemistry and Physics of Energetic Materials.* NATO ASI Series; Plenum: New York, 1990.

(3) Adams, G. F.; Shaw, R. W., Jr. *Annu. Rev. Phys. Chem.* **1992**, *43*, 311−340.

(4) Behrens, R., Jr.; Bulusu, S. *J. Phys. Chem.* **1992**, *96*, 8877−8897.

(5) Behrens, R. Chapter 14 in ref 2.

(6) Schroder, M. A. BRL-TR-2659 & BRL-TR-2673 (1985), and *Proceedings of the 177th JANNAF Combustion Meeting*, CPIA pub. #329, 1980.

(7) Iyer, S.; Eng, Y. S.; Joyce, M.; Perez, R.; Alster, J.; Stec, D. Report to the Am. Defence Preparations Assoc. April 1991.

(8) Oyumi, Y. Brill, T. B.; Rheingold, A. L.; Haller, T. M. *J. Phys. Chem.* **1985**, *89*, 4317.

(9) Zhang, Y.-X.; Yu, C.-L.; Bauer, S. H. *Int. J. Chem. Kinet.* **1998**, *30*, 185−191.

(10) Kamo, T.; Yamada, M.; Tang, J.; Ohshima, Y. *Nippon Kagaku Kaishi* **1987**, 1560−1566.

(11) Gardiner, W. C., Jr.; Walker, B. F.; Wakefield, C. B. In *Shock Waves in Chemistry*; Lifshitz, A., Ed.; Marcel Dekker Inc.: New York, 1981; Chapter 7.

(12) Mitchell, R. E.; Kee, R. J. A General-Purpose Computer Code for Predicting Chemical Behavior behind Incident and Reflected Shock Waves. Sandia Report, 1991.

(13) Behrens, R., Jr. Snadia Report, March 1994.

(14) Huffman, R. E.; Davidson, D. *J. Am. Chem. Soc.* **1959**, *81*, 2311.

(15) Zhang, Y.-X.; Bauer, S. H. *J. Phys. Chem. B* **1997**, *101*, 8717−8726.

(16)
Yu, C.-L.; Zhang, Y.-X.; Bauer, S. H. *J. Mol. Struct. (THEOCHEM)* **1998**, *432*, 63−68.

(17) Alchibald, T. G.; Gibardi, R. G.; Baum, K.; George, C. *J. Org. Chem.* **1990**, *55*, 2900.

(18) Archibald, T. G.; Garver, L. C.; Malik, A. A.; Bonsu, F. O.; Tzeng, D. D.; Preston, S. B.; Baum, K. Report ONR-2-10, Feb 1988.

(19) Thompson, C. A. Rice, J. K.; Russel, T. P.; Seminario, J. M.; Politzer, P. *J. Phys. Chem. A* **1997**, *101*, 7742−7748.

(20) Politzer, P.; Lane, P.; Grice, M. E.; Concha, M. C.; Redfern, P. C. *J. Mol. Struct. (THEOCHEM)* **1995**, *338*, 249.

(21) Anex, D. S.; Allman, J. C.; Lee, Y. T. In *Chemistry of Energetic Materials*; Olah, G. A., Squire, D. R., Eds.; Academic Press: New York, 1991; Chapter 2.

(22) Glandzer, K.; Troe, J. *Helv. Chim. Acta*. **1972**, *55*, 2884.

(23) Politzer, P.; Seminario, J. M. *Chem. Phys. Lett*. **1993**, *207*, 27.

(24) Oyumi, Y.; Brill, T. B. *Combust. Flame* **1985**, *62*, 225−231.

(25) (a) Oxley, J.; Smith, J.; Zheng, W.; Roger, E.; Coburn, M. *J. Phys. Chem. A* **1997**, *101*, 4375−4383. (b) Garland, N. L.; Nelson, H. H. *J. Phys. Chem. B* **1998**, *102*, 2663.

(26) (a) Melius, C. F. In *Chemistry and Physics of Energetic Materials*; Busulu, S. N., Ed.; Kluwer Academic Publisher: The Netherlands, 1990; pp 21−78. (b) Melius, C. F. *J. Phys. Colloq. C4*, **1987**, *48*, 34. (c) Melius, C. F.; Binkley, J. S. *Symp. (Int.) Combust*, **1986**, *21*, 1953.

(27) Wu, C.; Fried, L. E. *J. Phys. Chem. A* **1997**, *101*, 8675−8679.

(28) Dewar, M. J. S.; Ritchie, J. P. *J. Org. Chem*. **1985**, *50*, 1031−1036.

(29) Zhao, X. S.; Hintsa, E.; Lee, Y. T. *J. Chem. Phys*. **1988**, *88*, 801.

(30) (a) Nigenda, S. E.; McMillen, D. F.; Golden, D. M. *J. Phys. Chem*. **1989**, *93*, 1124−1130. (b) Stwart, P. H.; Jeffries, J. B.; Zellweger, J. M.; Golden, D. M. *J. Phys. Chem.* **1989**, *93*, 3557−3563.

(31) Krodzicki, M.; Seminario, J. M.; Politzer, P. *Theor. Chim. Acta* **1990**, *77*, 359−367.